Published in final edited form as:
*Circ Cardiovasc Genet*. 2014 June ; 7(3): 257–265. doi:10.1161/CIRCGENETICS.113.000455.

# A Point Mutation in *Myh10* Causes Major Defects in Heart Development and Body Wall Closure

**Xuefei Ma, PhD** and **Robert S. Adelstein, MD**
Laboratory of Molecular Cardiology, National Heart, Lung, and Blood Institute, National Institutes of Health, Bethesda, MD

## Abstract

**Background—**The three isoforms of nonmuscle myosin II (NMII-A, NMII-B and NMII-C) play various roles during mouse embryonic development. Previous work, using knockout and hypomorphic mice, showed that MYH10 encoding myosin heavy chain II-B is critical for cardiac and brain development. Ablating or decreasing NMII-B by 80% results in cardiac (ventricular septal defect, double outlet of the right ventricle) and brain defects but not midline fusion defects. Neither NMII-A nor II-C appear to play roles in early myocardial development.

**Methods and Results—**We had previously generated point mutant knock-in mice and now report novel findings due to expressing motor deficient NMII-B at wild-type levels. Homozygous mice die at E14.5 in cardiac failure exhibiting abnormalities not seen in NMII-B null and hypomorphic mice: a failure in midline fusion resulting in a cleft palate, ectopia cordis, and a large omphalocele. Fusion of the sternum and endocardial cushions is impaired in the mutant mice associated with a failure in apoptosis of the mesenchyme cells. Failure to disassemble myocyte cell-cell adhesions during cardiac outflow tract development contributes to impaired outflow tract myocardialization and displacement of the aorta to the right ventricle.

**Conclusions—**Expression of motor impaired NMII-B disrupts normal ventral body wall closure, due to a dominant negative effect. This is not due to the loss of NMII-B function but rather to a gain-of-function resulting from prolonged crosslinking of NMII-B to actin-filaments thereby interfering with the dynamics of actomyosin cytoskeletal structure. Moreover impaired NMII-B motor activity inhibits outflow tract myocardialization leading to mis-localization of the aorta.

### Keywords

Nonmuscle Myosin II; Outflow Tract; Apoptosis; Ventral Body Wall Closure; MYH10

## Introduction

Nonmuscle myosin (NM) II plays important roles in various cellular processes including cell migration, cell morphology, cytokinesis and cell-cell adhesion.[1] Three different NMII heavy

**Correspondence:** Dr. Xuefei Ma National Institutes of Health Building 10, Room 6C-104 10 Center Drive, MSC 1583 Bethesda, MD 20892-1583 Tel: (301) 402-1993 Fax: (301) 402-1582 MaX@nhlbi.nih.gov.

**Conflict of Interest Disclosures:** None.

chains (NMHCs) are expressed and encoded by three different genes, Myh9[2, 3] 10[2] and 14[4, 5]. The protein products are referred to as NMHCII-A, II-B and II-C, respectively and mutations in NMHCII-A[6, 7] and NMHCII-C[8, 9] cause a number of human syndromes. To study how a mutation in NMII-B could affect pathophysiological processes in vivo, we mutated Arg709 to Cys in the motor domain of NMHCII-B in mice ($B^{R709C}/B^{R709C}$). This amino acid, and the surrounding residues are conserved in all myosin II family members, including skeletal, cardiac and smooth muscle myosin.

To understand the effect of the R709C mutation on NMII-B activity, we previously characterized a baculovirus expressed heavy meromyosin (HMM) fragment, R709C-HMMII-B, which contains the NMII enzymatic and actin-binding domains.[10] R709C-HMMII-B showed two important changes in biological properties compared to wild-type HMMII-B: a 70% decrease in its actin-activated MgATPase activity and a complete loss in its ability to propel actin-filaments in an *in vitro* motility assay. Furthermore the R709C-HMMII-B displayed an increased affinity for actin and spent a prolonged period bound to actin-filaments during cross-bridge cycling.[11]

As part of generating $B^{R709C}/B^{R709C}$ mice using homologous recombination we inserted the neomycin cassette for selection of the mutant embryonic stem cells into the *Myh10* intron, 5' of exon 16, thus initially producing hypomorphic mice ($B^{R709CN}/B^{R709CN}$) that expressed a decreased (20%) amount of the mutant NMII-B. These mice developed cardiac and brain abnormalities similar to NMII-B null ($B^{-}/B^{-}$) mice, although the onset of the abnormalities was delayed compared to the knockouts.[12, 13] Somewhat surprisingly when we removed the cassette encoding neomycin resistance thereby increasing the expression of mutant NMII to wild-type levels, the hydrocephalus and defects in myocyte cytokinesis were rescued, although the abnormalities in neuronal cell migration were not.[11, 14] We interpreted these results as showing that NMII has two distinct functions *in vivo*: a structural-scaffolding function that is important for cell-cell adhesion and relies on the ability of NMII to form bipolar filaments which cross-link actin. This would explain the ability of the mutant NMII-B and other isoforms to rescue the defect in cell adhesion in the neuroepithelial cells lining the spinal canal, which causes the hydrocephalus.[14] In contrast, the inability of the mutant NMII-B to rescue the neuronal migration defects was thought to reflect the defect in the mutant NMII-B motor activity as measured by the decreased MgATPase activity and the loss of *in vitro* motility, a property unique to each isoform.

In the present report we characterize the novel abnormalities found in $B^{R709C}/B^{R709C}$ and $B^{+}/B^{R709C}$ mice which differ significantly from $B^{-}/B^{-}$ and hypomorphic mice. These include a major defect in midline fusion resulting in a cleft palate (homozygotes only), *ectopia cordis* (homozygotes only), and an omphalocele containing the liver and intestines, diaphragmatic herniation, and structural cardiac abnormalities (homozygotes only), defects similar to those first described in humans by Cantrell.[15]

## Materials and Methods

### NMHCII-B mutant Mice

$B^{-}/B^{-}$, $B^{R709CN}/B^{R709CN}$ and $B^{R709C}/B^{R709C}$, $B^{a*}/B^{a*}$ mice were generated as previously described[12, 16, 17] and are available through the Mutant Mouse Regional Resource Centers (MMRRC, #16991, #16142, #15983, and #16998). $B^{-}/B^{-}$, $B^{R709CN}/B^{R709CN}$, and $B^{a*}/B^{a*}$ mice are maintained in a mixed background of 129/Sv and C57BL/6. All procedures were conducted using an approved animal protocol in accordance with National Heart, Lung, and Blood Institute Animal Care and Use Committee.

### Histology and Immunofluorescence Staining

Staining was performed as described.[12] Primary antibodies (Table S1) for immunostaining were incubated at 4°C overnight following antigen retrieval in 10mM citrate buffer (pH 6). The confocal images were collected using a Zeiss LSM 510-META. In all cases when possible comparison was made among littermates. For each genotype we analyzed at least 5 mice.

### TUNEL Assay

The TUNEL assay was carried out using the In Situ Cell Death Detection Fluorescein Kit, following the manufacturer's instructions (Roche Applied Science).

### Statistical Analyses

Data are expressed as mean ± SD. The Student's t-test was performed to compare two means. A One-Way Analysis of Variance (ANOVA) was used to compare three or more means at one time. Data passed normality test for statistical analysis.

## Results

### Defects in Ventral Wall Closure in $B^{R709C}/B^{R709C}$ and $B^{+}/B^{R709C}$ Mice

The $B^{R709C}/B^{R709C}$ mice die during embryonic development between E14.5 to E16.5. As shown in Figure 1b, E14.5 $B^{R709C}/B^{R709C}$ mice developed generalized edema (white arrow), indicating a major failure in cardiac function. Figure S1b shows evidence for massive congestive failure in the liver of $B^{R709C}/B^{R709C}$ mice indicated by the presence of sinusoidal dilatation, focal hemorrhages and congestion (compare to wild type, Figures 1a, S1a). Measurements of cardiac function using *in utero* echocardiography at E14.5 showed a marked decrease in fractional shortening (FS) and heart rate (HR) and an increase in the left ventricular dimension in systole (LVDs) in $B^{R709C}/B^{R709C}$ embryos (Table S2). $B^{R709C}/B^{R709C}$ embryos develop an umbilical hernia (Figure 1b, orange arrow), indicating a failure in ventral body wall closure. Figures 1c,d show sagittal sections of E13.5 embryos from $B^{+}/B^{R709C}$ and $B^{R709C}/B^{R709C}$ embryos. In both cases the liver is abnormally herniated outside the body (arrows). Approximately 50% of $B^{+}/B^{R709C}$ mice and all $B^{R709C}/B^{R709C}$ mice develop an omphalocele. Furthermore, ~50% of $B^{R709C}/B^{R709C}$ mice develop *ectopia cordis*, with the heart protruding outside the thoracic chamber (Figure 1f, black arrow). *Ectopia cordis* was not seen in $B^{+}/B^{R709C}$ mice, suggesting that the severity of the defects in ventral body wall closure is dependent on the dosage of mutant NMII-B.

$B^{R709C}/B^{R709C}$ embryos also develop cleft palates. At E14.5, the left and right palatal shelves of $B^{+}/B^{+}$ mice are positioned in a horizontal plane above the tongue and are joined (Figure 1g, arrow). In contrast, the $B^{R709C}/B^{R709C}$ palatal shelves are much shorter, positioned vertically, and flank the tongue with a major gap between them (Figure 1h, arrows). This defect does not appear to be due to a delay in development of $B^{R709C}/B^{R709C}$ embryos. Those few $B^{R709C}/B^{R709C}$ embryos that survive to E16.5 still show cleft palates (Figure S2).

## Congenital Diaphragmatic Hernia in Heterozygous and Homozygous NMII-B Mutant Mice

$B^{R709C}/B^{R709C}$ and $B^{+}/B^{R709C}$ mice show abnormal development of the diaphragm which leads to herniation of the liver into the thoracic cavity. Figures 2a-c show sagittal sections of the developing diaphragm of $B^{+}/B^{+}$, $B^{+}/B^{R709C}$, and $B^{R709C}/B^{R709C}$ mice at E13.5 stained with antibodies to NMHCII-A (green) and striated muscle myosin (MF20, red). The skeletal muscle cells of $B^{+}/B^{+}$ mice are uniformly distributed throughout the entire dorsal area of the diaphragm (a, red; yellow and white boxes, enlarged in d,g). However in both $B^{+}/B^{R709C}$ (b) and $B^{R709C}/B^{R709C}$ (c) mice, skeletal muscle cells accumulate abnormally in the central region (white boxes in b and c, enlarged in h,i,). This results in significantly fewer muscles cells at the most lateral region of the diaphragm (yellow boxes in b and c, enlarged in e,f) consistent with a defect in migration of the skeletal muscle cells. To quantify the distribution of muscle cells we divided the diaphragm into three equal segments: ventral, middle and lateral, and calculated the percentages of muscle cells for each segment from 3 mice of each genotype. These values are: 38.5±1.3%, 30.3±1.8% and 31.1±1.2% for ventral, middle, and lateral segments respectively in the $B^{+}/B^{+}$ diaphragm; 56.2±1.3%, 38.1± .5%, and 5.8±1.7% respectively in the $B^{+}/B^{R709C}$ diaphragm; and 57.9±1.5%, 41.7±1.2%, 0.43±0.3% respectively in the $B^{R709C}/B^{R709C}$ diaphragm. Statistical analysis shows a significant increase in muscle cells in the ventral segments and a significant reduction in the lateral segments of $B^{+}/B^{R709C}$ and $B^{R709C}/B^{R709C}$ compared to the $B^{+}/B^{+}$ diaphragm (ANOVA, $p<0,05$). The absence of muscle cells makes this part of the diaphragm vulnerable to herniation. Since the ventral body wall is wide open in $B^{R709C}/B^{R709C}$ mice, the diaphragmatic hernia is more easily observed in $B^{+}/B^{R709C}$ mice (Figure S3b,c). The amuscular lateral region of the diaphragm of an E19.5 $B^{+}/B^{R709C}$ mouse becomes very thin permitting the liver to protrude into the thoracic cavity (Figure S3b, black arrow). Figure S3a shows an equivalent section from a control E19.5 $B^{+}/B^{+}$ embryo. Figure S3c shows a 2 month old $B^{+}/B^{R709C}$ mouse, which did not develop an obvious omphalocele but still developed a severe diaphragmatic hernia which permitted the intestines to protrude into the thoracic cavity. The lack of muscle cells in the lateral regions of the mutant diaphragms is not associated with increased apoptosis, since no obvious apoptotic cells were observed in the developing diaphragms from the three genotypes.

Importantly, none of the defects described above with respect to midline fusion are seen in $B^{-}/B^{-}$, or $B^{R709CN}/B^{R709CN}$ mice.[12, 16] The midline fusion defects are unlikely to be due to background strain differences in these mouse lines. Both $B^{+}/B^{R709C}$ and $B^{-}/B^{R709C}$, but not $B^{+}/B$- offspring from $B^{+}/B^{-}$ and $B^{+}/B^{R709C}$ crosses developed defects in ventral body wall closure. We next studied the cellular mechanisms underlying these defects.

## Impaired Apoptosis in the Fusing Sternum of $B^{R709C}/B^{R709C}$ Mice

*Ectopia cordis* is usually associated with defects in sternal fusion.[18] In $B^+/B^+$ mice at E14.5, the fusing halves of the lower sternum are aligned side by side (Figure1e, green arrow). In $B^{R709C}/B^{R709C}$ mice they are widely separated (Figure 1f, green arrows; Figure 3d, inset). To understand the cellular mechanisms underlying this defect, we examined apoptotic activity in the fusing sternum of E14.5 $B^+/B^+$ and $B^{R709C}/B^{R709C}$ mice. Most of the $B^+/B^+$ sternal mesenchymal cells are undergoing apoptosis manifested by nuclear condensation and fragmentation (Figure 3a, arrows). In contrast, very few apoptotic cells were found in the same area in $B^{R709C}/B^{R709C}$ mice (Figure 3b). TUNEL assays confirmed the apoptosis in $B^+/B^+$ sternums (Figure 3c, green), which was decreased in $B^{R709C}/B^{R709C}$ mice (Figure 3d, green). The percent of apoptotic mesenchymal cells in $B^+/B^+$ and $B^{R709C}/B^{R709C}$ sternums was 14.4±7.7% and 1.4±0.8% ($p<0.001$, t-test), respectively (n=5 mice for each genotype). Previous studies from cultured cells have shown that NMII is required for the final stages of apoptosis.[19-21] We next examined a step in the upstream pathway, activation of caspase-3, using immunostaining for activated-caspase-3. In $B^+/B^+$ mice, a significant number of mesenchymal cells (46.2±7.2%) in the fusing sternum were positive for activated caspase-3 (Figure 3e, red), whereas very few mesenchymal cells (5.4±2.3%, n=5 mice each genotype, $p<0.001$, t-test) stained positively for activated caspase-3 in the $B^{R709C}/B^{R709C}$ sternum (Figure 3f, red). We then examined these same cells for expression of p53, the signaling molecule that initiates apoptosis. There were no major difference in p53 expression in $B^{R709C}/B^{R709C}$ sternal mesenchymal cells compared to $B^+/B^+$ mesenchymal cells (Figure 3e,f, green). The relative average fluorescence intensities of p53 staining from $B^+/B^+$ and $B^{R709C}/B^{R709C}$ sternums were 52.8±1.5% and 61.9±5.3% (n=3 mice each, $p>0.05$, t-test). These results indicate that NMII-B functions upstream of capase-3 but downstream of p53 in regulating mesenchymal cell apoptosis of the fusing sternum. The requirement for enzymatic NMII activity in apoptosis has been reported in various cell types in culture. We further asked which enzymes are responsible for activation of NMII during sternal fusion. We examined the expression of myosin light chain kinase (MLCK) and Rho-kinase (ROCK1) in the fusing sternum and found that ROCK1, but not MLCK is expressed (Figure S4). Thus ROCK1 mediated NMII activation is most likely involved in normal sternum fusion, although further investigation is required to test this hypothesis.

## Sternal Mesenchymal Cells Express both NMII-A and II-B But Not NMII-C

It has previously been reported that dorsal wall closure in *Drosophila* (corresponding to mammalian ventral wall closure) requires zipper, the sole *Drosophila* NMII isoform.[22] However mice and humans express three different isoforms of NMII. We therefore examined the expression patterns of NMII-A, II-B and II-C in the developing mouse sternum. Figure 3g-i shows immunofluorescence confocal images for NMII-A, II-B and II-C from an E14.5 wild-type mouse embryo. Both NMII-A (g) and II-B (h), but not II-C (i) were detected in mesenchymal cells of the developing sternums. Previous reports have demonstrated that ablation of NMII-B did not impair ventral body wall closure in mice,[16] indicating that expression of NMII-A alone is sufficient to support ventral body wall closure. Importantly, despite normal expression of NMIIA, expression of R709C-NMII-B leads to defects in ventral body wall closure. Since these defects did not occur in $B^-/B^-$

mice, they are unlikely the result of loss of NMII-B function. This raises the possibility that in $B^{R709C}/B^{R709C}$ mice, the mutant NMII-B isoform is interfering with the normal function of NMII-A during sternal fusion.

## Failure in Fusion and Remodeling of the Atrioventricular Cushions in $B^{R709C}/B^{R709C}$ Mouse Hearts

$B^{R709C}/B^{R709C}$ mouse hearts show defects in fusion and remodeling of the atrioventricular (AV) endocardial cushions which are not seen in $B^{-}/B^{-}$ or wild-type hearts. Figures 4a-i show the developing AV valves of $B^{+}/B^{+}$, $B^{R709C}/B^{R709C}$ and $B^{-}/B^{-}$ mouse hearts from E11.5 to E14.5. At E11.5, prior to the fusion of the superior and inferior cushions, no differences in shape, size and positioning of the cushions were found among $B^{+}/B^{+}$ (a), $B^{R709C}/B^{R709C}$ (b) and $B^{-}/B^{-}$ (c) hearts, suggesting a normal endothelial-mesenchymal transition (EMT) in developing $B^{R709C}/B^{R709C}$ and $B^{-}/B^{-}$ hearts. At E12.5 the $B^{+}/B^{+}$ AV cushions have fused and started to elongate (d). In contrast the $B^{R709C}/B^{R709C}$ cushions have not fused and show no sign of elongation (e). By E14.5 $B^{+}/B^{+}$ AV cushions have developed into elongated, mature mitral (MV) and tricuspid (TV) valves (g). The superior and inferior cushions of $B^{R709C}/B^{R709C}$ mice are still not fused or remodeled (h), suggesting that the defects in $B^{R709C}/B^{R709C}$ AV cushions are not simply due to a delay in development. In $B^{-}/B^{-}$ hearts, the AV cushions were fused normally at E12.5 (Figure 4f). However the maturation into cardiac valves is delayed at E14.5 (Figure 4i) at the time $B^{-}/B^{-}$ mice start to die.

Similar to its role in sternal formation, apoptosis also plays an important role in the development of the endocardial AV cushions. We next investigated whether apoptosis was impaired in the developing $B^{R709C}/B^{R709C}$ endocardial cushions using TUNEL assays. At E12.5, fusion of the superior and inferior cushions in $B^{+}/B^{+}$ hearts was accompanied by significant numbers of apoptotic mesenchymal cells (Figure 4j, green, 11.2±3.0%). However, very few apoptotic cells were detected in $B^{R709C}/B^{R709C}$ cushions at E12.5 which fail in fusion (Figure 4k, 1.1±0.9%, n=5 mice each genotype, $p<0.001$, t-test). Note that at E11.5, no obvious apoptotic cells were detected in either $B^{+}/B^{+}$ or $B^{R709C}/B^{R709C}$ AV cushions (Figure S5a,b). Moreover, we did not observe obvious apoptotic cells in $B^{R709C}/B^{R709C}$ cushions at E14.5 (Figure S5d), suggesting that the defect in apoptosis is not due to a developmental delay in the $B^{R709C}/B^{R709C}$ mouse heart. These results emphasize the role of NMII in apoptosis. Similar to the developing sternum, mesenchymal cells in developing AV cushions express NMII-A (Figure S6a, green) and II-B (Figure S6b, green), but no detectable II-C (Figure S6c). These results are consistent withthe hypothesis that mutant NMII-B interferes with the normal function of NMII-A in $B^{R709C}/B^{R709C}$ cardiac AV cushion development. This is also consistent with our findings that NMII-B/II-C doubly ablated mice showed no defect in ventral wall closure or in AV cushion fusion.[23]

## Defects in Outflow Tract Myocardialization in $B^{R709C}/B^{R709C}$ and $B^{-}/B^{-}$ Mouse Hearts

Both $B^{-}/B^{-}$[16] and $B^{R709C}/B^{R709C}$ hearts showed defects in outflow tract (OFT) alignment with both the aorta and pulmonary artery emanating from the right ventricle (DORV; Figure 5a-c; 10 out of 10 $B^{R709C}/B^{R709C}$ mice). During heart development, the OFT cardiac cushions are initially composed of cardiac jelly. Following invasion by endocardial cells and

cardiac neural crest cells, the cushions expand, fuse and consequently form a mesenchymal outlet septum. The mesenchyme of the proximal region of the outlet septum is then replaced by cardiac myocytes during a process called myocardialization.[24] In mice, the invasion by cardiac myocytes occurs between E10.5 to E13.5. Figure 5d,e shows H&E stained images of developing hearts at E11.5 illustrating the invasion by the cardiac myocytes of the $B^+/B^+$ cardiac cushion (Figure 5d, arrow), but absence of invasion in $B^{R709C}/B^{R709C}$ mice (Figure 5e, arrow). During this process, the cardiac myocytes from the outer layer of myocardium in the OFT lose their tight cell-cell adhesions, become polarized and migrate into the adjacent cushions. Inhibition of myocardialization leads to abnormal alignment of the OFT.[24] Therefore we examined myocardialization in the OFTs of wild-type and $B^{R709C}/B^{R709C}$ mice using immunofluorescence confocal microscopy with antibodies to MF20 to delineate the cardiac myocytes, and antibodies to NMHCII-B to identify both cardiac myocytes and cardiac non-myocytes. Figure 5f shows that at E11.5, the $B^+/B^+$ myocardial cells bordering the OFT are polarized, with extended lamellipodia- and filopodia-like structures protruding into the adjacent mesenchymal cells of the cushions (Figure 5f, arrows, and S7a). However in $B^{R709C}/B^{R709C}$ mice there is a discrete boundary between the OFT myocardium and the cushion since the cardiac myocytes remain compact with no sign of invasion (Figure 5g and S7b).

Next we looked for the cause of the failure of migration in the $B^{R709C}/B^{R709C}$ myocytes. Since phosphorylation of the regulatory myosin light chain (MLC20) is required for activation of NMII, we used antibodies to the two most likely kinases that are known to phosphorylate MLC20, ROCK1 and MLCK, to see if they were present in the OFT and whether their pattern of expression was altered in the $B^{R709C}/B^{R709C}$ OFT. Figure S7a,b show that ROCK1 is present in the cardiac myocytes in the OFT of both $B^+/B^+$ and $B^{R709C}/B^{R709C}$ mice. This kinase is not detected in the ventricular myocytes (Figure S7 c.d). In contrast MLCK was detected in the OFT and ventricular myocytes of both the normal and mutant mice (Figure S8). Figure S7e,f shows that MLC20 is phosphorylated in both wild-type and $B^{R709C}/B^{R709C}$ cardiac myocytes. This makes it unlikely that the failure in migration is due to a lack of MLC20 phosphorylation or alteration in the ROCK1 or MLCK expression and suggests that the defect in myocyte migration entails an intrinsic kinetic property of the mutant NMII-B.

We sought a mechanism related to the kinetic properties of the mutant and wild-type NMII to explain the defect in migration in $B^{R709C}/B^{R709C}$ cardiac myocytes. Previous work has shown that the disassembly of cell-cell adhesion junctions requires NMII activity.[25, 26] Examination of the cell-cell adhesion boundaries in the myocytes of the OFT by immunofluorescence confocal microscopy showed marked differences between $B^+/B^+$ and $B^{R709C}/B^{R709C}$ cardiac myocytes. Figure 5i (arrows) shows that the cell adhesion molecule N-cadherin (the only classical cadherin expressed in the myocardium) is concentrated at the cell-cell boundary of the cardiac myocytes in the $B^{R709C}/B^{R709C}$ OFT. This indicates that the $B^{R709C}/B^{R709C}$ cardiac myocytes retain tight cell-cell adhesions. In contrast, there is no cortical concentration of N-cadherin in the actively migrating $B^+/B^+$ cardiac myocytes at E11.5 (Figure 5h). These results suggest that the mutation R709C, which decreases NMII-B MgATPase activity and increases the time NMII-B spends bound to actin, inhibits the

disassembly of cell-cell adhesions in the cardiac myocytes. This results in a failure in myocardialization, thereby contributing to the development of the DORV.

The aorta of $B^{-}/B^{-}$ hearts is also abnormally localized to the right ventricle as previously reported.[16] Figure 6 shows that similar to the $B^{R709C}/B^{R709C}$ OFT, the $B^{-}/B^{-}$ OFT shows defects in myocardialization (Figure 6c) and disassembly of cardiac myocyte cell-cell adhesions (Figure 6d) compared to a $B^{+}/B^{+}$ littermate (Figure 6a,b). Since normal alignment of the aorta is impaired in $B^{R709C}/B^{R709C}$ as well as in $B^{-}/B^{-}$ hearts these findings suggest a requirement for wild-type NMII-B enzymatic motor activity in these processes during normal mouse heart development. This is also consistent with our finding that genetic replacement of NMII-B with NMII-A does not rescue the DORV[17] because of the defects of OFT myocardialization (Figure S9).

## Discussion

Table 1 summarizes the phenotypes observed from our three NMII-B genetically altered mouse models. The findings from these mutant mice have resulted in two hypotheses with respect to the mechanism underlying the NMII-B mutation: The first is that the novel gain-of-function defects found in these mice are due to interference of the R709C-NMII-B with the normal function of a second NMII, NMII-A. The second is that the mechanism underlying these defects arises from the two different functions of the NMII-B molecule: the motor function and the structural function.

Evidence that the mutant NMII-B is interfering with the normal function of NMII-A during ventral wall closure or endocardial cushion fusion is as follows: hypomorphic $B^{R709CN}/B^{R709CN}$ mice, mice ablated for NMII-B or II-C or mice doubly ablated for II-B and II-C show normal closure of the ventral body wall and normal endocardial cushion fusion. Therefore expression of NMII-A alone is sufficient for ventral body wall development. In addition these defects are also observed in the $B^{R709C}/B^{R709C}$ homozygous mice, which do not contain any normal NMII-B, so interference with the normal isoform of NMII-B is not possible. Moreover the two affected tissues do express significant amounts of NMII-A (but not NMII-C). This raises the novel possibility that the mutant NMII-B is interfering with NMII-A. *In vitro* motility studies using baculovirus-expressed NMII-A HMM and mutant NMII-B HMM showed that the presence of the R709C NMII-B HMM markedly slowed the movement of NMII-A HMM.[10] Mechanistically, prolonged binding of R709C NMII-B to actin-filaments[11] could affect the dynamics of actomyosin stress fibers[27] which in general contain both NMII-A and NMII-B[28]. It is of interest that there have been several reports implicating a mutation in NMII-A[29-31] but not NMII-C[32] in the generation of a cleft palate in humans, consistent with our hypothesis that the mutant II-B is interfering with II-A. Of course we cannot rule out interference with a nonmuscle myosin of a different class.

Previous work has shown that NMII-A ablated mice die at E6.5 and the heterozygous IIA mice are entirely normal[33] so we cannot directly test our hypothesis. However in support of this mechanism is our finding of a significant gene dose-dependent effect: All $B^{R709C}/B^{R709C}$ mutant mice are severely affected, showing abnormalities including cleft palate, *ectopia cordis* (50%) and omphalocele. Approximately one-half of $B^{+}/B^{R709C}$ mice,

expressing 50% mutant NMII-B compared to wild-type mice, are born with an omphalocele only, and hypomorphic mice ($B^{R709CN}/B^{R709CN}$) expressing only 25% mutant myosin display neither defect.

The requirement for NMII function in ventral body wall closure is also supported by results from ROCK ablated mice, which show a failure in body wall closure associated with a deficiency in the formation of actomyosin bundles in the umbilical ring.[34] In a chick model for defective ventral body wall closure this abnormality was attributed to reduced myosin activity due to decreased ROCK expression.[35] In both cases the defects are similar to our $B^{+}/B^{R709C}$ mice but much milder compared to $B^{R709C}/B^{R709C}$ mice. This is most likely due to a partial inactivation of NMII function in ROCK ablated mice since other kinases are also capable of activating NMII.[1]

Our second hypothesis is that the defects we observed in $B^{R709C}/B^{R709C}$ mice arise from two distinct, though not unrelated functions of myosin: NMII can utilize either its enzymatic motor domain to translocate actin-filaments or NMII can act more as a structural protein to cross-link actin-filaments. Both of these functions require the binding of myosin to actin, however translocation of actin requires a particular isoform-specific, actin-activated MgATPase activity and duty cycle (amount of time the myosin head stays bound to actin) in order to perform a normal functional role in motile processes such as cell migration. These functions of NMII are more sensitive to mutations that alter kinetic properties and cannot be rescued by other NMII isoforms with different motors and kinetic properties.[17] An example of this is generation of the DORV in the $B^{R709C}/B^{R709C}$ mice in which the mutant NMII-B cannot dissociate the cell-cell adhesion complex nor can it participate in migration of the myocytes into the cardiac cushion. We postulate that the result of this inability to migrate normally into the cardiac cushion is mis-localization of the aortic root to the right ventricle. Of note is a report by Phillips et al. attributing the development of a DORV to abnormalities in NMII function.[36] Another example of defective migration is found in the mutant skeletal muscle cells of the developing diaphragm resulting in diaphragmatic herniation. An additional consequence of the NMII-B motor mutation is the apparent failure of the cardiac and sternal mesenchymal cells to undergo a normal apoptotic program. The loss of apoptosis results in abnormal valve formation as well as a defect in sternal fusion, two novel defects not seen in NMII-B ablated or hypomorphic mice.

Mice either ablated for NMII-B or expressing R709C-NMII-B, either in reduced (25%) or wild-type amounts, develop abnormalities in myocardialization during cardiac OFT development leading to misalignment of the aorta with the right ventricle. Our results indicate that both the expression level and the normal enzymatic activity of NMII-B are essential for normal OFT myocardialization. MLCK and ROCK are two of the major kinases which activate NMII activity. Specific expression of ROCK1 in OFT cardiac myocytes during myocardialization suggests that ROCK1 is the major upstream kinase activating NMII-B. This is supported by findings from Loop-tail (Lp) mice where abnormal OFT myocardialization is associated with disruption of noncanonical Wnt, planar cell polarity mediated RhoA/ROCK1 signaling.[36] Decreased expression of ROCK1 in the proximal OFT cardiac myocytes was also described in Cx43 knockout mice which developed DORV with abnormal OFT myocardialization.[37] Since no changes in ROCK1

expression and NMII activation (MLC20 phosphorylation) were observed in the $B^{R709C}$/$B^{R709C}$ OFT, we attribute the defects in myocardialization directly to the impaired R709C-NMII-B enzymatic activity. Our results further point to the importance of NMII-B mediated disruption of cardiac myocyte cell-cell contacts during OFT myocardialization. Cardiac myocytes lose their epithelial context and migrate into the adjacent mesenchymal cushions during myocardialization. Expression of R709C-NMII-B in mice prevents OFT cardiac myocytes from detaching from surrounding cells and the retention of cell-cell adhesions thereby inhibits their migration into the cushion tissue. Loss of the NMII enzymatic activity and prolonged binding of the mutant NMII to actin contribute to the inability of R709C-NMII-B to disrupt cell-cell adhesions. This is consistent with the requirement for NMII activity to perturb pre-existing epithelial cell-cell adhesions in culture.[38, 39] All of the above evidence is consistent with a Wnt/RhoA/ROCK1/NMII-B pathway in regulating myocardialization during OFT development. Abnormal outflow tract alignment is one of the most common congenital heart defects. Defects in OFT myocardialization appear to be the common end pathway leading to this abnormality.

During revision of this manuscript Dr. Wendy Chung's group reported a patient carrying a nonsense mutation resulting in a premature stop codon in the MYH10 transcript.[40] Among various abnormalities, the patient developed congenital diaphragmatic hernia which is one of the defects of Pentalogy of Cantrell and is seen in our NMII-B mutant mice reported here. Our present plans call for testing our hypothesis by searching for possible mutations in NMII-B and related proteins in patients with the diagnosis of Pentalogy of Cantrell.

## Supplementary Material

Refer to Web version on PubMed Central for supplementary material.

## Acknowledgments

We thank Dr. Mary Anne Conti for her significant contributions to this manuscript. Dr. Sachiyo Kawamoto and members of the Laboratory of Molecular Cardiology also provided critical comments on the manuscript. We also thank Dr. Kazuyo Takeda for echocardiography. Drs. Chengyu Liu and Yubin Du (National Heart, Lung, and Blood Institute [NHLBI] Transgenic Core) and Drs. Christian A. Combs and Daniela Malide (NHLBI Light Microscopy Core) provided outstanding service and advice. Antoine Smith and Dalton Saunders provided technical assistance.

**Funding Sources:** This research was supported by the Division of Intramural Research, NHLBI.

## References

1. Vicente-Manzanares M, Ma X, Adelstein RS, Horwitz AR. Non-muscle myosin II takes centre stage in cell adhesion and migration. Nat Rev Mol Cell Biol. 2009; 10:778–790. [PubMed: 19851336]
2. Simons M, Wang M, McBride OW, Kawamoto S, Yamakawa K, Gdula D, et al. Human nonmuscle myosin heavy chains are encoded by two genes located on different chromosomes. Circ Res. 1991; 69:530–539. [PubMed: 1860190]
3. Toothaker LE, Gonzalez DA, Tung N, Lemons RS, Le Beau MM, Arnaout MA, et al. Cellular myosin heavy chain in human leukocytes: Isolation of 5′ cdna clones, characterization of the protein, chromosomal localization, and upregulation during myeloid differentiation. Blood. 1991; 78:1826–1833. [PubMed: 1912569]

4. Golomb E, Ma X, Jana SS, Preston YA, Kawamoto S, Shoham NG, et al. Identification and characterization of nonmuscle myosin II-C, a new member of the myosin ii family. J Biol Chem. 2004; 279:2800–2808. [PubMed: 14594953]
5. Leal A, Endele S, Stengel C, Huehne K, Loetterle J, Barrantes R, et al. A novel myosin heavy chain gene in human chromosome 19q13.3. Gene. 2003; 312:165–171. [PubMed: 12909352]
6. Burt RA, Joseph JE, Milliken S, Collinge JE, Kile BT. Description of a novel mutation leading to myh9-related disease. Thromb Res. 2008; 122:861–863. [PubMed: 18676005]
7. Seri M, Pecci A, Di Bari F, Cusano R, Savino M, Panza E, et al. Myh9-related disease: May hegglin anomaly, sebastian syndrome, fechtner syndrome, and epstein syndrome are not distinct entities but represent a variable expression of a single illness. Medicine (Baltimore). 2003; 82:203–215. [PubMed: 12792306]
8. Donaudy F, Snoeckx R, Pfister M, Zenner HP, Blin N, Di Stazio M, et al. Nonmuscle myosin heavy-chain gene myh14 is expressed in cochlea and mutated in patients affected by autosomal dominant hearing impairment (dfna4). Am J Hum Genet. 2004; 74:770–776. [PubMed: 15015131]
9. Yang T, Pfister M, Blin N, Zenner HP, Pusch CM, Smith RJ. Genetic heterogeneity of deafness phenotypes linked to dfna4. Am J Med Genet A. 2005; 139:9–12. [PubMed: 16222661]
10. Kim KY, Kovacs M, Kawamoto S, Sellers JR, Adelstein RS. Disease-associated mutations and alternative splicing alter the enzymatic and motile activity of nonmuscle myosins II-B and II-C. J Biol Chem. 2005; 280:22769–22775. [PubMed: 15845534]
11. Ma X, Kovacs M, Conti MA, Wang A, Zhang Y, Sellers JR, et al. Nonmuscle myosin II exerts tension but does not translocate actin in vertebrate cytokinesis. Proc Natl Acad Sci. USA. 2012; 109:4509–4514. [PubMed: 22393000]
12. Ma X, Kawamoto S, Hara Y, Adelstein RS. A point mutation in the motor domain of nonmuscle myosin II-B impairs migration of distinct groups of neurons. Mol Biol Cell. 2004; 15:2568–2579. [PubMed: 15034141]
13. Takeda K, Kishi H, Ma X, Yu ZX, Adelstein RS. Ablation and mutation of nonmuscle myosin heavy chain II-B results in a defect in cardiac myocyte cytokinesis. Circ Res. 2003; 93:330–337. [PubMed: 12893741]
14. Ma X, Bao J, Adelstein RS. Loss of cell adhesion causes hydrocephalus in nonmuscle myosin II-B-ablated and mutated mice. Mol Biol Cell. 2007; 18:2305–2312. [PubMed: 17429076]
15. Cantrell JR, Haller JA, Ravitch MM. A syndrome of congenital defects involving the abdominal wall, sternum, diaphragm, pericardium, and heart. Surg Gynecol Obstet. 1958; 107:602–614. [PubMed: 13592660]
16. Tullio AN, Accili D, Ferrans VJ, Yu ZX, Takeda K, Grinberg A, et al. Nonmuscle myosin II B is required for normal development of the mouse heart. Proc Natl Acad Sci USA. 1997; 94:12407–12412. [PubMed: 9356462]
17. Bao J, Ma X, Liu C, Adelstein RS. Replacement of nonmuscle myosin II-B with II-A rescues brain but not cardiac defects in mice. J Biol Chem. 2007; 282:22102–22111. [PubMed: 17519229]
18. Engum SA. Embryology, sternal clefts, ectopia cordis, and cantrell's pentalogy. Semin Pediatr Surg. 2008; 17:154–160. [PubMed: 18582820]
19. Gerashchenko BI, Murata-Hori M, Hosoya H. Myosin regulatory light chain as a critical substrate of cell death: A hypothesis. Med Hypotheses. 2000; 54:850–852. [PubMed: 10859700]
20. Mills JC, Stone NL, Erhardt J, Pittman RN. Apoptotic membrane blebbing is regulated by myosin light chain phosphorylation. J Cell Biol. 1998; 140:627–636. [PubMed: 9456322]
21. Solinet S, Vitale ML. Isoform b of myosin II heavy chain mediates actomyosin contractility during tnfalpha-induced apoptosis. J Cell Sci. 2008; 121:1681–1692. [PubMed: 18445680]
22. Young PE, Richman AM, Ketchum AS, Kiehart DP. Morphogenesis in drosophila requires nonmuscle myosin heavy chain function. Genes Dev. 1993; 7:29–41. [PubMed: 8422986]
23. Ma X, Jana SS, Conti MA, Kawamoto S, Claycomb WC, Adelstein RS. Ablation of nonmuscle myosin II-B and II-C reveals a role for nonmuscle myosin ii in cardiac myocyte karyokinesis. Mol Biol Cell. 2010; 21:3952–3962. [PubMed: 20861308]
24. van den Hoff MJ, Moorman AF, Ruijter JM, Lamers WH, Bennington RW, Markwald RR, et al. Myocardialization of the cardiac outflow tract. Dev Biol. 1999; 212:477–490. [PubMed: 10433836]

25. Sahai E, Marshall CJ. Rock and dia have opposing effects on adherens junctions downstream of rho. Nat Cell Biol. 2002; 4:408–415. [PubMed: 11992112]
26. Sturge J, Wienke D, Isacke CM. Endosomes generate localized rho-rock-mlc2-based contractile signals via endo180 to promote adhesion disassembly. J Cell Biol. 2006; 175:337–347. [PubMed: 17043135]
27. Vicente-Manzanares M, Zareno J, Whitmore L, Choi CK, Horwitz AF. Regulation of protrusion, adhesion dynamics, and polarity by myosins IIA and IIB in migrating cells. J Cell Biol. 2007; 176:573–580. [PubMed: 17312025]
28. Wei Q, Adelstein RS. Conditional expression of a truncated fragment of nonmuscle myosin II-A alters cell shape but not cytokinesis in hela cells. Mol. Bio. Cell. 2000; 11:3617–3627. [PubMed: 11029059]
29. Birnbaum S, Reutter H, Mende M, de Assis NA, Diaz-Lacava A, Herms S, et al. Further evidence for the involvement of myh9 in the etiology of non-syndromic cleft lip with or without cleft palate. Eur J Oral Sci. 2009; 117:200–203. [PubMed: 19320731]
30. Chiquet BT, Hashmi SS, Henry R, Burt A, Mulliken JB, Stal S, et al. Genomic screening identifies novel linkages and provides further evidence for a role of myh9 in nonsyndromic cleft lip and palate. Eur J Hum Genet. 2009; 17:195–204. [PubMed: 18716610]
31. Martinelli M, Di Stazio M, Scapoli L, Marchesini J, Di Bari F, Pezzetti F, et al. Cleft lip with or without cleft palate: Implication of the heavy chain of non-muscle myosin IIA. J Med Genet. 2007; 44:387–392. [PubMed: 17337617]
32. Martinelli M, Arlotti M, Palmieri A, Scapoli L, Savoia A, Di Stazio M, et al. Investigation of myh14 as a candidate gene in cleft lip with or without cleft palate. Eur J Oral Sci. 2008; 116:287–290. [PubMed: 18471249]
33. Conti MA, Even-Ram S, Liu C, Yamada KM, Adelstein RS. Defects in cell adhesion and the visceral endoderm following ablation of nonmuscle myosin heavy chain II-A in mice. J Biol Chem. 2004; 279:41263–41266. [PubMed: 15292239]
34. Shimizu Y, Thumkeo D, Keel J, Ishizaki T, Oshima H, Oshima M, et al. Rock-i regulates closure of the eyelids and ventral body wall by inducing assembly of actomyosin bundles. J Cell Biol. 2005; 168:941–953. [PubMed: 15753128]
35. Doi T, Puri P, Bannigan J, Thompson J. Downregulation of Rock-I and Rock-II gene expression in the cadmium-induced ventral body wall defect chick model. Pediatr Surg Int. 2008; 24:1297–1301. [PubMed: 18956198]
36. Phillips HM, Murdoch JN, Chaudhry B, Copp AJ, Henderson DJ. Vangl2 acts via rhoa signaling to regulate polarized cell movements during development of the proximal outflow tract. Circ Res. 2005; 96:292–299. [PubMed: 15637299]
37. Qi CH, Zhao XQ, Ma D, Ma XJ, Zhou GM, Huang GY. Downregulation of rho associated coiled-coil forming protein kinase 1 in the process of delayed myocardialization of cardiac proximal outflow tract septum in connexin 43 knockout mice embryo. Chin Med J. (Engl). 2011; 124:2021–2027. [PubMed: 22088464]
38. Ivanov AI, Parkos CA, Nusrat A. Cytoskeletal regulation of epithelial barrier function during inflammation. Am J Pathol. 2010; 177:512–524. [PubMed: 20581053]
39. Ivanov AI, McCall IC, Parkos CA, Nusrat A. Role for actin filament turnover and a myosin ii motor in cytoskeleton-driven disassembly of the epithelial apical junctional complex. Mol Biol Cell. 2004; 15:2639–2651. [PubMed: 15047870]
40. Tuzovic L, Yu L, Zeng W, Li X, Lu H, Lu HM, et al. A human de novo mutation in myh10 phenocopies the loss of function mutation in mice. Rare Diseases. 2013; 1:e26144–26141-e26144-26145. [PubMed: 25003005]

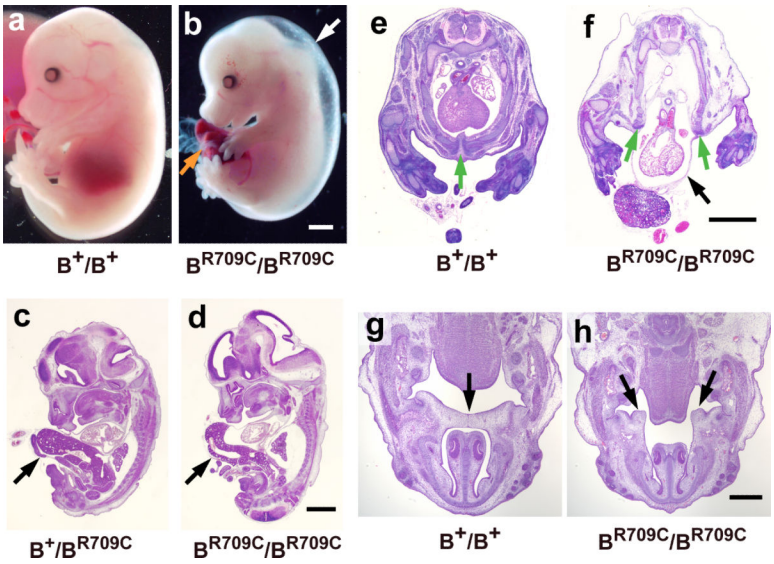


**Figure 1.**

Congestive Heart Failure and Midline Fusion Defects in $B^{R709C}/B^{R709C}$ Mice. a,b. Representative images of wild-type ($B^{+}/B^{+}$, a) and $B^{R709C}/B^{R709C}$ (b) mice at E14.5 showing generalized edema (white arrow) and an umbilical hernia (orange arrow) in a $B^{R709C}/B^{R709C}$ mouse. c,d. H&E stained sagittal sections of E13.5 embryos show a herniated liver in $B^{+}/B^{R709C}$ (c, arrow) and $B^{R709C}/B^{R709C}$ (d, arrow) mice. e,f. H&E stained cross sections of E14.5 embryos show *ectopia cordis* in a $B^{R709C}/B^{R709C}$ mouse (f, black arrow). A similar section from a $B^{+}/B^{+}$ mouse is shown in panel e. In 50% of $B^{R709C}/B^{R709C}$ mice, the two halves of the lower sternum are widely separated (f, green arrows; compare to e, green arrow) allowing the heart to protrude outside the thoracic chamber. g,h. H&E stained cross sections of E14.5 embryos show a cleft palate in a $B^{R709C}/B^{R709C}$ mouse (h, arrows). In the $B^{+}/B^{+}$ section (g) the two palatal shelves contact each other (arrow). Scale bars: a-f, 1 mm; g and h, 500 μm.

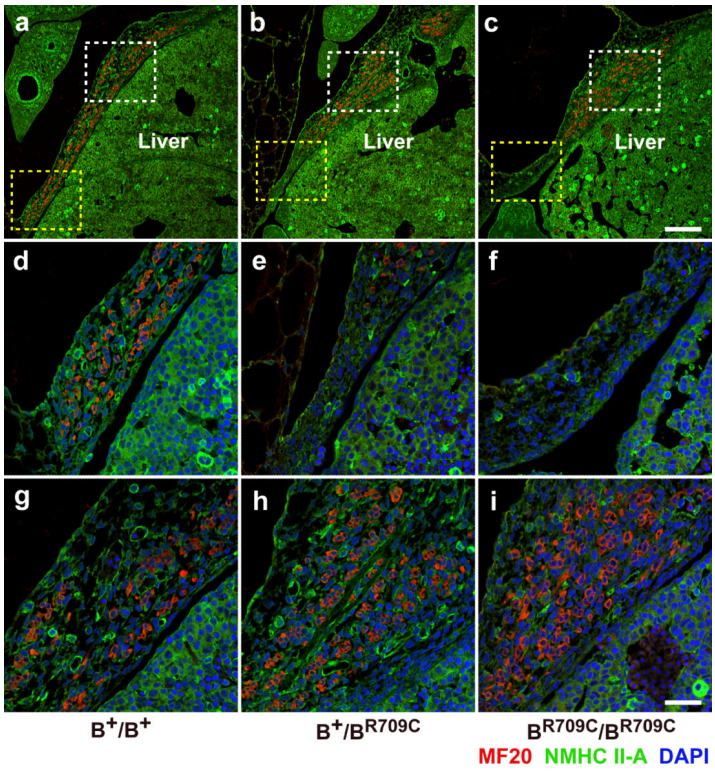


**Figure 2.**

Defects in Diaphragm Development in $B^{+}/B^{R709C}$ and $B^{R709C}/B^{R709C}$ embryos. a-i. Immunofluorescence confocal images of E13.5 mouse sagittal sections near the middle of the torso stained for NMHCII-A (green) and striated muscle myosin (MF20, red) show loss of skeletal muscle cells in the lateral-most region of the diaphragm in $B^{+}/B^{R709C}$ and $B^{R709C}/B^{R709C}$ embryos (b,c, yellow boxes; enlarged in e,f). In the $B^{+}/B^{+}$ embryo skeletal muscle cells are numerous in this region (a, yellow box; enlarged in d). Skeletal muscle cells accumulated near the midline of the $B^{+}/B^{R709C}$ and $B^{R709C}/B^{R709C}$ diaphragm (b,c, white boxes; enlarged in h,i) compared to the $B^{+}/B^{+}$ diaphragm (a, white box; enlarged in g). DAPI (blue) stains nuclei. Scale bars: a-c, 200 μm; d-i, 50 μm.

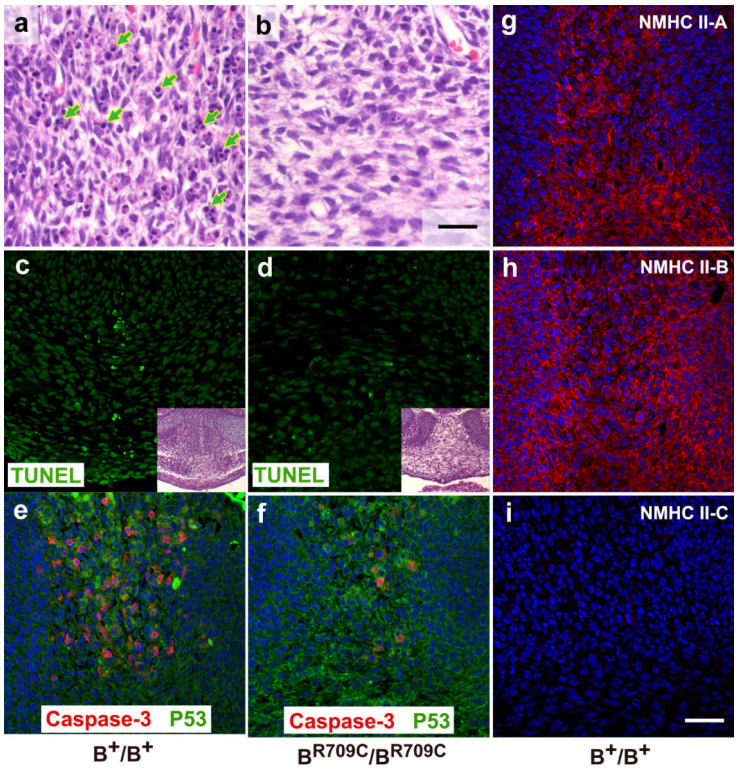


**Figure 3.**

Impaired Apoptosis in the Fusing Lower Sternum of $B^{R709C}/B^{R709C}$ Embryos. a,b. H&E stained mesenchymal cells in the middle of the E14.5 fusing sternum show an extensive accumulation of apoptotic cells with condensed and/or fragmented chromosomes in $B^{+}/B^{+}$ mice (a, green arrows). Very few apoptotic cells are seen in $B^{R709C}/B^{R709C}$ mice (b). c,d. Confocal images of TUNEL assays show apoptotic cells near the midline in the fusing sternum of $B^{+}/B^{+}$ mice (c, green) which are not seen in $B^{R709C}/B^{R709C}$ mice (d). The insets (H&E images) indicate areas shown in panels c and d. e,f. Confocal images of the sternal area stained with antibodies for activated-caspase-3 (red) and p53 (green) from E14.5 mouse embryos show a decrease in caspase-3 positive cells in $B^{R709C}/B^{R709C}$ mice (f, red) compared to $B^{+}/B^{+}$ mice (e, red). No difference in p53 staining was seen between $B^{+}/B^{+}$ and $B^{R709C}/B^{R709C}$ mice (e,f, green).g-i. Confocal images of E14.5 mouse embryos stained with antibodies for NMHCII-A (g, red), II-B (h, red) and II-C (i) show that both NMHCII-A and II-B, but not II-C, are expressed in the fusing sternum. DAPI (blue) stains nuclei. Scale bars: a and b, 25 μm; c-i, 50 μm.

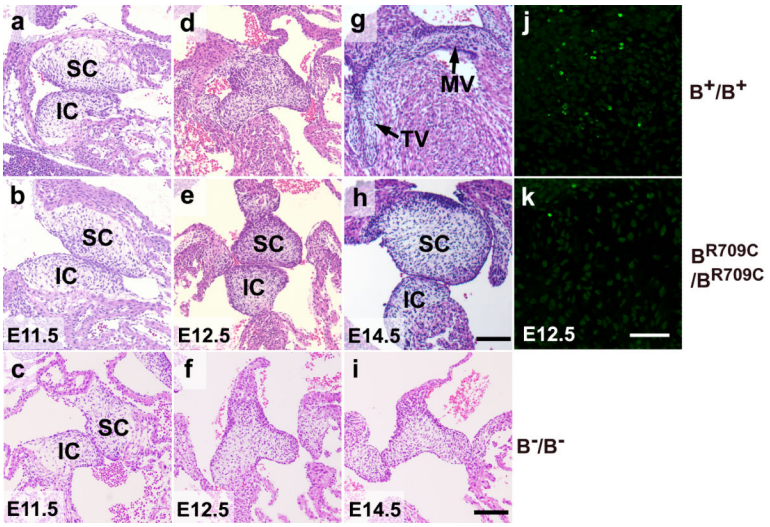


**Figure 4.**

Defects in Fusion and Remodeling of the Atrioventricular Cushions in $B^{R709C}/B^{R709C}$ Mouse Hearts. a-i. H&E stained heart sections of $B^{+}/B^{+}$, $B^{R709C}/B^{R709C}$, and $B^{-}/B^{-}$ embryos show developmental progression of atrioventricular (AV) cushions from E11.5 to E14.5. E11.5 AV cushions show no differences in size, morphology and positioning between $B^{+}/B^{+}$ (a), $B^{R709C}/B^{R709C}$ (b) and $B^{-}/B^{-}$ (c) hearts. $B^{+}/B^{+}$ AV cushions fuse and start to elongate at E12.5 (d), and acquire mature mitral (MV) and tricuspid (TV) valve leaflets by E14.5 (g). $B^{R709C}/B^{R709C}$ cushions remain unfused and show no sign of maturation at E12.5 (e) and E14.5 (h). The fusion of AV cushions in $B^{-}/B^{-}$ hearts appears normal at E12.5 (f), however further maturation into cardiac valves is delayed at E14.5 (i) compared to the $B^{+}/B^{+}$ mouse (e). IC, inferior AV cushion; SC, superior AV cushion. j,k. TUNEL assay shows defective apoptosis in developing $B^{R709C}/B^{R709C}$ cushions. Apoptotic cells are readily seen in $B^{+}/B^{+}$ cushions (j, green), but very few apoptotic cells are found in $B^{R709C}/B^{R709C}$ cushions (k). DAPI (blue) stains nuclei. Scale bar: a-i, 40 μm; j,k, 25μM.

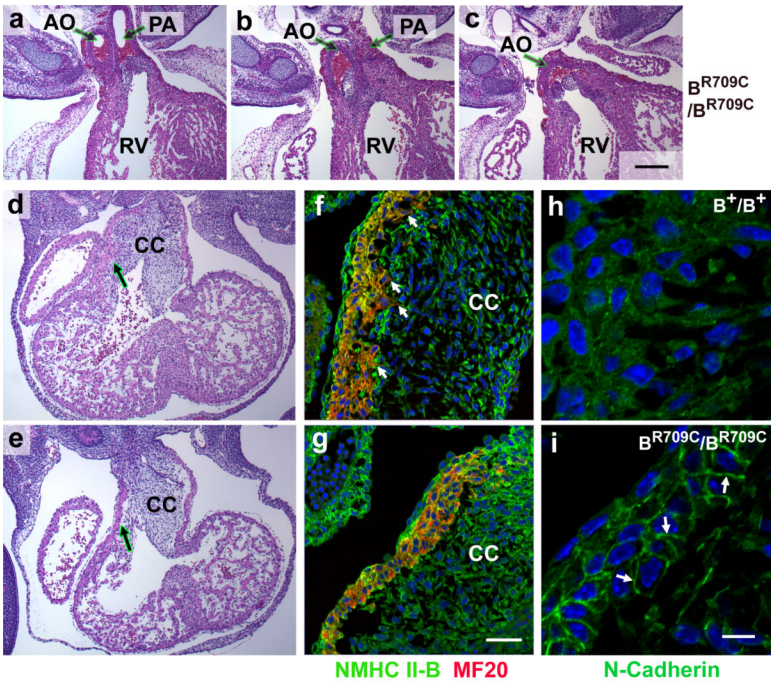


**Figure 5.**

Defective Myocardialization of Developing Outflow Tract in $B^{R709C}/B^{R709C}$ Mouse Hearts. a-c. Serial H&E stained heart sections from an E14.5 $B^{R709C}/B^{R709C}$ embryo show abnormal configuration of the great arteries with DORV. AO, aorta; PA, pulmonary artery; RV, right ventricle. d,e. H&E stained sections of E11.5 mouse hearts show that the cardiac myocytes in the developing OFT are invading the underlying cardiac cushions (CC) in the $B^{+}/B^{+}$ mouse heart (d, arrow) but not in the $B^{R709C}/B^{R709C}$ heart (e, arrow). f,g. Immunofluorescence confocal microscope images of the OFT from E11.5 mouse hearts stained with antibodies for NMHCII-B (green) and MF20 (red, marker for sarcomeric myosin indicating cardiac myocytes) show that the $B^{+}/B^{+}$ cardiac myocytes are invading the cardiac cushion (f, small arrows), but the $B^{R709C}/B^{R709C}$ myocytes are not (g). h,i. Immunofluorescence images of the developing OFT from E11.5 mouse hearts stained with antibodies for N-cadherin (green) show that in the $B^{+}/B^{+}$ OFT there is no obvious enrichment of N-cadherin at the boundaries between cardiac myocytes (h). In contrast, in the $B^{R709C}/B^{R709C}$ myocytes, N-cadherin is enriched at the cell-cell boundaries (i, arrows). DAPI (blue) stains nuclei. Scale bars: a-e, 200 μm; f and g, 50 μm; h and i, 10 μm.

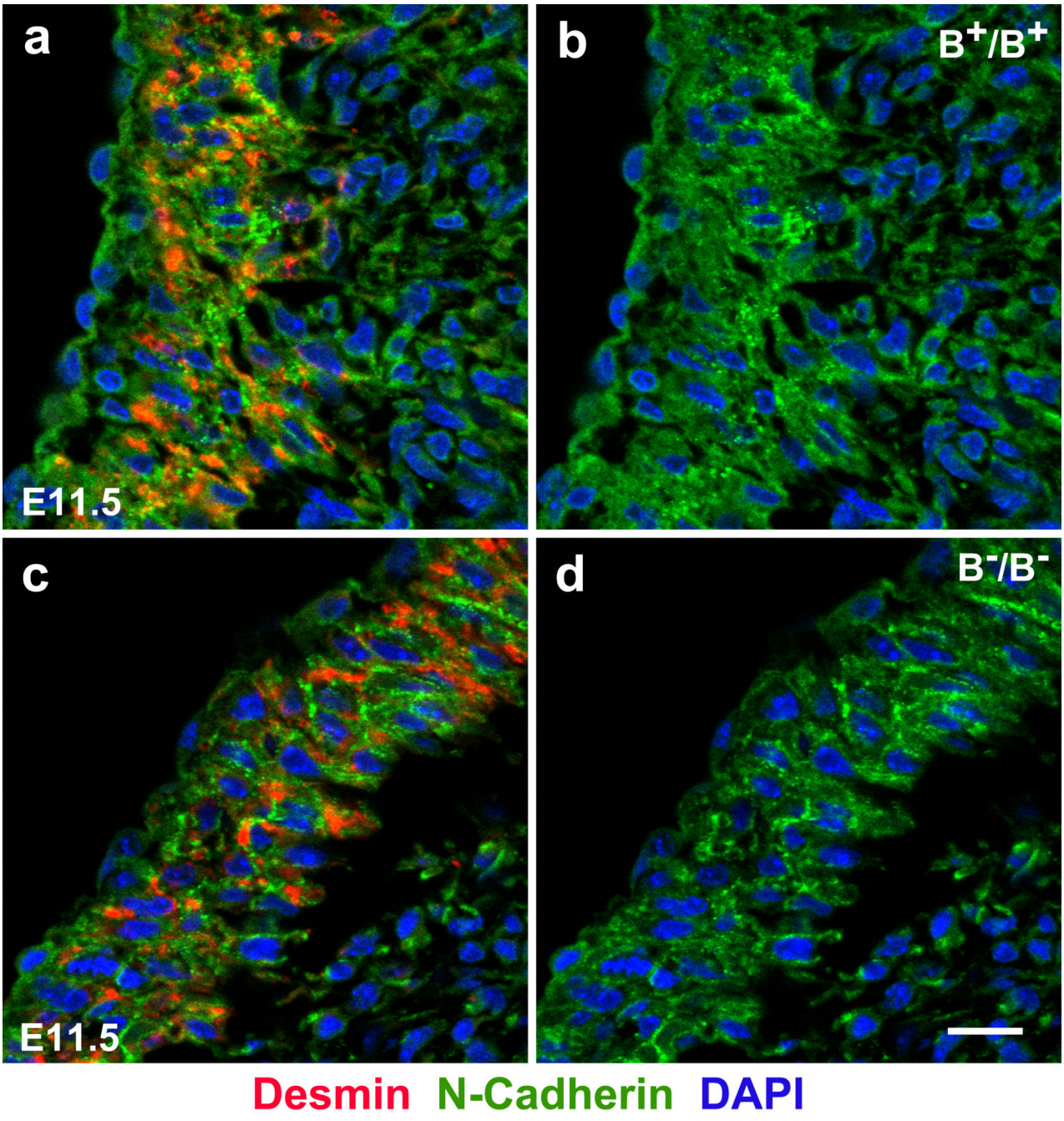


**Figure 6.**

Defective Myocardialization of the Developing Outflow Tract in $B^{-}/B^{-}$ Mouse Hearts. a-d. Immunofluorescence confocal microscope images of E11.5 mouse cardiac outflow tracts stained with antibodies for desmin (a,c red, a marker for cardiac myocytes) or N-cadherin (a-d, green). N-cadherin localization shows that the cardiac myocytes are invading the underlying cardiac cushions in the $B^{+}/B^{+}$ mouse heart (a, red) but not in the $B^{-}/B^{-}$ heart (c, red) causing a defect in OFT myocardialization in $B^{-}/B^{-}$ mouse hearts. Staining of the cardiac intercellular adhesion molecule N-cadherin shows that in the $B^{+}/B^{+}$ OFT there is no

obvious localization of N-cadherin at the boundaries between cardiac myocytes (a,b, green). In $B^{-}/B^{-}$ OFT, N-cadherin is localized at the cell-cell boundaries (c,d, green) indicating a failure in disassembly of cardiac myocyte cell-cell adhesions. Scale bars: 10 μm.

## Table 1

Phenotypes of NMII-B knockout and R709C mutant Mice

| | Brain | Heart | Body Wall |
|---|---|---|---|
| **$B^+/B^+$, $B^+/B^-$, $B^+/B^{R709CN}$** | None | None | None |
| **$B^-/B^-$** | Hydrocephalus, Abnormal neuronal migration, Disruption of neuroepithelial cell adhesion | Defect in cardiac myocyte cytokinesis, Decreased proliferation or early exit from mitosis of cardiac myocytes, Double outlet of right ventricle, Ventricular septal defect | None |
| **$B^{R709CN}/B^{R709CN}$** | Hydrocephalus, Abnormal neuronal migration, Disruption of neuroepithelial cell adhesion, Delayed cerebellum development | Defect in cardiac myocyte cytokinesis, Decreased proliferation and early exit from mitosis of cardiac myocytes, Double outlet of right ventricle, Ventricular septal defect | None |
| **$B^+/B^{R709C}$** | None | None | Omphalocele (50%), Diaphragmatic herniation |
| **$B^{R709C}/B^{R709C}$** | Abnormal neuronal migration | Decreased proliferation and early exit from mitosis of cardiac myocytes, Double outlet of right ventricle, Ventricular septal defect, Defects in fusion and remodeling of the endocardiac cushions, Ectopia cordis (50%). | Cleft palate, Split lower sternum, Omphalocele, Diaphragmatic herniation |

We have analyzed at least 10 mice for each genotype. The phenotypes seen in mutant mice are 100% penetrant except as indicated.